This document is confidential and is proprietary to the American Chemical Society and its authors. Do not copy or disclose without written permission. If you have received this item in error, notify the sender and delete all copies.

Polymer Conformations and Diffusion Through a Monolayer of Confining Nanoparticles

Journal:	*Macromolecules*
Manuscript ID	ma-2020-01524w.R1
Manuscript Type:	Article
Date Submitted by the Author:	30-Aug-2020
Complete List of Authors:	Bailey, Eric; University of Pennsylvania School of Engineering and Applied Science, Materials Science and Engineering Riggleman, Robert A.; University of Pennsylvania, Chemical and Biomolecular Engineering Winey, Karen; University of Pennsylvania, Materials Science and Engineering Department

SCHOLARONE™
Manuscripts

Polymer Conformations and Diffusion Through a Monolayer of Confining Nanoparticles

Eric J. Bailey[1], Robert A. Riggleman[2], and Karen I. Winey*[1,2]

[1]Department of Materials Science and Engineering and [2]Department of Chemical and Biomolecular Engineering, University of Pennsylvania, Philadelphia, Pennsylvania 19104, United States

*Author to whom correspondence should be addressed. Electronic address: winey@seas.upenn.edu

For Table of Contents use only:

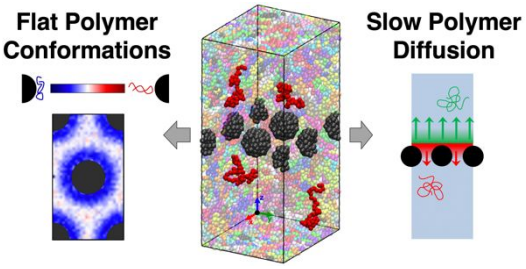

Abstract

We present coarse-grained molecular dynamics simulations to probe chain-scale polymer conformations and diffusion between confining nanoparticles (NPs). By constructing a monolayer of hexagonally-packed NPs in a polymer melt with athermal interactions, we observe the magnitude and length-scale over which homogeneously confining NPs impact the polymer behavior, which provides fundamental insights into more complex polymer nanocomposites. We show that polymer conformations are more perturbed under strong confinement (i.e. when the interparticle distance, ID, is less than twice the polymer radius of gyration, $2R_g$) as compared to around an isolated NP, and the effect depends on the ratio of R_{NP}/R_g rather than either independently. In fact, these conformations can be quantitatively replicated by executing a simple random walk in a similarly confining environment. We also show that polymer diffusion is slowed by the presence of NPs and the slowing persists far beyond the length-scale over which polymer conformations are perturbed. Although the slowing is strongest ~R_g from the NPs, the diffusion coefficient is slower even beyond ~$5R_g$ from the NPs. Furthermore, by analyzing the directional van Hove distributions, we show polymer diffusion away from the NP monolayer is bulk-like while diffusion through the monolayer is slower with increasing NP confinement. These molecular dynamics simulations provide fundamental insights into the temporal and spatial effect of confining, athermal NPs on chain-scale polymer conformations and diffusion.

Introduction

It is well known that static and dynamic properties of a polymer melt can be altered by the addition of nanoparticles (NPs).[1–4] These hybrid materials, called polymer nanocomposites (PNCs), have received considerable attention for several decades due to their potential applications in critical areas such as electronics, biomedical engineering, and energy.[3,4] Despite the diverse research through experiments, simulations, and theory, the connection between microscopic parameters and macroscopic properties remains elusive, motivating the need for further fundamental studies.[4,5] The conformations and dynamics of polymer chains near NPs influence the mechanical, transport, and functional properties and more broadly, the processability of PNCs. However, due to the broad and interrelated parameter space and complex nature of PNC materials, the NP-induced perturbation to static and dynamic properties is not well established.

The experimental determination of polymer chain conformations (e.g. the radius of gyration, R_g) in PNCs with small angle scattering is challenging. Using small angle neutron scattering (SANS), experimental observations of increased chain dimensions,[6] decreased chain dimensions,[7] and unperturbed conformations[8] have been reported, as more thoroughly compiled recently[9]. In one contribution, meticulous fitting of combined X-ray and neutron scattering revealed an interfacial layer in attractive PNCs over which the structure (e.g. density, conformations, chain packing) are perturbed, but individual chain conformations were unavailable.[7] In part due to the ensemble-averaging and isotropic nature of PNCs and SANS, molecular dynamics simulations are more conducive for detailed interrogation of polymer conformations, as reviewed recently.[10] Starr et al. used MD simulations of a single faceted NP in a polymer melt to show polymer chain flattening at the NP surface (for $R_{NP} > R_g$) and the recovery of bulk conformations beyond ~R_g from the NP surface.[11,12] Other authors have conducted similar simulations in the dilute regime with various NP sizes, chain lengths, NP-polymer interactions, and reported expanded[12–17] and mostly unperturbed[18–20] conformations with all conformations within ~20% of bulk. Fewer simulations have addressed strongly-confined PNCs (high

NP concentration) that include several NPs in the simulation box placed with either random order or a lattice.[21,22] For example, for a variety of NP sizes (R_g/R_{NP} ~ 1-8), repulsive NPs did not perturb the average polymer conformations, but chain swelling was observed with increasing loading of small, attractive, NPs.[22] In part due to the often conflicting results and dense parameter space, a mechanistic understanding of how NPs perturb polymer conformations, especially under strong confinement, is missing.

The dynamics of polymer chains are also known to be perturbed near NPs. It is reasonably well-established by the convergence of simulations and experiments on different material systems and methods that small length-scale polymer segmental dynamics are slow near attractive and weakly interacting NPs.[1,4,23–26] At longer length-scales, the chain-scale polymer diffusion is known to be affected by the presence of NPs. Elastic recoil detection (ERD) has been used to measure tracer polymer diffusion into PNCs with spherical NPs for various NP concentrations, tracer MWs, NP sizes (R_{NP}), and NP-polymer interactions.[27–31] In each case, the polymer diffusion coefficient was slower in the PNC (D) than in bulk (D_0), and in each system, D/D_0 was found to depend on the confinement parameter ($ID/2R_g$) where ID is the average accessible interparticle distance between nearest NPs. Furthermore, $D/D_0 < 1$ was observed even at $ID/2R_g \sim 10$, which implies that the temporal impact of NPs on polymer diffusion is spatially long-lasting. Note that deviations from this behavior, where D/D_0 is related to $ID/2R_g$, has been observed as a function of temperature[32] and in PNCs with more mobile NPs.[33]

Although MD simulations of polymer diffusion can be challenging due to computational expense, especially for high NP loadings and long polymer chains, insights have been gained from MD simulations and other calculations, as recently reviewed.[34] For example, the addition of attractive NPs was found to slow polymer diffusion relative to bulk as a function of NP concentration.[18] However, a nonmonotonic trend was observed in PNCs with repulsive NPs where $D/D_0 > 1$ at low NP concentrations and $D/D_0 < 1$ when tortuosity dominates at higher NP concentrations.[18] In another set

of MD simulations, polymer diffusion was found to be reduced relative to bulk with increasing NP concentration and the slowing was more significant than predicted by tortuosity.[35] More recently, scaling of D/D_0 with $ID/2R_g$, similar to experimental observations, was observed in dynamic Monte Carlo simulations but a scaling factor that depends on temperature, NP size, and NP-polymer interaction was needed to collapse the various PNC systems.[36] Furthermore, the convergence of $D/D_0 \sim 1$ occurred at $ID/2R_g \sim 3$ which is much more rapid than observed in experimental systems. Despite numerous observations, a systematic understanding of how D/D_0 depends on $ID/2R_g$ and the origin of the spatially long-lasting effect of NPs on polymer diffusion remains unclear.

In this article, we use coarse-grained molecular dynamics simulations to study polymer conformations between weakly and highly confining NPs and to probe the spatial and temporal impact of a monolayer of NPs on polymer diffusion. By placing a monolayer of hexagonally packed NPs in a dense polymer melt we isolate the confined region and observe the transition from bulk-polymer behavior to confined behavior. In doing so, we systematically provide fundamental insights to the more complex PNC environment. We show that polymer conformations under strong confinement ($ID/2R_g < 1$) are more impacted than around an isolated NP, and the effect depends on the ratio of R_{NP}/R_g rather than either R_{NP} or R_g independently. Interestingly, these conformations are quantitatively replicated by executing a simple random walk in a similarly confining environment. We then show the perturbation to polymer diffusion is impacted far beyond the region over which polymer conformations are perturbed. We show the local polymer diffusion coefficient at $\sim R_g$ from the NPs is slowed as a function of confinement, and the slowing persists to more than $\sim 5R_g$ from the NPs. Furthermore, by analyzing the directional van Hove distributions, we show polymer preferentially diffuses away from the NP monolayer and diffusion through the monolayer is slowed as a function of confinement. The functional form (D/D_0 versus $ID/2R_g$) observed experimentally in bulk PNCs is also found in these monolayer systems of NPs, although the suppression to polymer diffusion is expectedly weaker with only a single, organized layer NPs as opposed to a random arrangement of many NPs in experimental PNCs. These

molecular dynamics simulations highlight the impact of a monolayer of NPs and provide fundamental insights into the temporal and spatial influence of NP-confinement on polymer conformations and diffusion.

Simulation Method

We conduct coarse grained molecular dynamics (MD) simulations that follow the well-established Kremer-Grest model.[37] The units reported herein are normalized to the monomer size (σ), potential strength (ε), and monomer mass (m) where time, $\tau = \sigma(m/\varepsilon)^{1/2}$. All simulations were run with the LAMMPS MD simulation package using the velocity-Verlet algorithm[38] in an NVT ensemble with the Langevin thermostat and periodic boundaries applied in all dimensions.

The NPs in these simulations were constructed from an amorphous melt of non-bonded monomer beads with density (ρ) of 0.9 σ^{-3}. All beads beyond R_{NP} from the center of the simulation were discarded leaving a spherical NP with amorphous bead structure and an effective radius approximately equal to the defined $R_{NP.}$ These NPs were then assembled into a hexagonal lattice monolayer in the x-y plane. The minimum interparticle distance (ID) is used to define the separation of nearest neighbor NPs, whose centers are displaced by ID+2R_{NP} (Figure 1a). While this defines the x and y dimensions of the box, the z-dimension was typically at least 10 R_g to incorporate a sufficient volume of bulk-like polymer. Box dimensions and other relevant parameters are listed in Table S1. Finally, polymer chains were added to the simulation box on a lattice above and below the NP monolayer and the system was equilibrated, as described below. The precise value of the z dimension was adjusted to achieve a polymer monomer density far from the NP monolayer of 0.85 σ^{-3}. A representative snapshot of the simulation box after equilibration and showing only four chains is presented in Figure 1b.

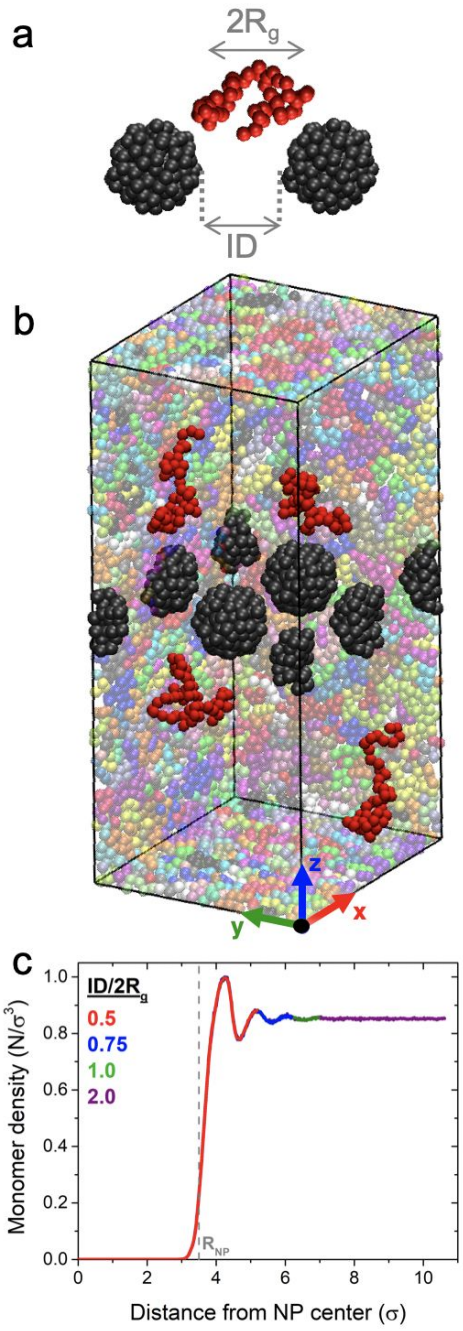

Figure 1: (a) Representative NPs and a polymer chain showing the interparticle distance (ID). (b) The simulation box with a monolayer of NPs (dark grey, $2R_{NP} = 7\sigma$, $ID/2R_g = 1.0$) and polymer chains (various colors, N = 50) with four representative chains highlighted (red). (c) Monomer density profile from the NP for similar monolayers systems at $ID/2R_g = 0.5 – 2$, N=50, and $2R_{NP} = 7\sigma$.

All nonbonded monomer-monomer interactions are governed by a repulsive Lennard-Jones (LJ) potential and bonded monomers are connected via a FENE anharmonic spring potential. Beads in the NP interact with polymer monomers through the same repulsive LJ potential as nonbonded monomers, making this an athermal system. A spring force was independently applied to NP beads, fixing their equilibrium position but allowing them to vibrate to prevent artificial crystallization caused by peaks and valleys on the NP surface. This makes the center-of-mass of the NPs immobile throughout the simulation, which is a reasonable approximation when $R_{NP} \sim R_g$ because NP diffusion is ~100 times slower than polymer diffusion in experimental systems.[4,27,29,39]

Equilibration of the system was monitored by conformation and dynamic properties of the polymer. For regions $>5R_g$ from the NP monolayer, monomer density and polymer conformations (R_g) were found to equilibrate to bulk values rapidly ($<\sim 10^5\ \tau$). During equilibration, the average monomer travelled $>>2R_g$ and reached the diffusive regime where MSD ~ t. For systems with N=200, equilibration was assisted by a bond swap algorithm followed by standard MD for times sufficient for full chain diffusion. For experimental sampling, a Langevin thermostat was used at T = 1 and the timestep used was 0.002τ for N=50 and 0.006τ for N=200.

Most results discussed in this work are systems with N=50 beads per polymer chain ($R_g = 3.6\sigma$) and NPs with $2R_{NP} = 7\sigma$ ($R_g/R_{NP} \sim 1$). However, in certain cases, systems with N=200 ($R_g \sim 7.2\sigma$) and $2R_{NP} = 3.5\sigma$ and 14σ are also reported. In general, we explore levels of confinement of $ID/2R_g = 0.5$, 0.75, 1, and 2 as well as bulk polymer. The NP-polymer interface in each system with N=50 and $2R_{NP}=7\sigma$ can be observed by the monomer density profile versus the distance from the NP center, Figure 1c. Due to the amorphous surface structure and lightly vibrating beads, there is slight monomer penetration within R_{NP} on the order of $\sim 0.5\sigma$. In addition, density fluctuations away from the NP surface are minimal and independent of degree of confinement. Analysis of polymer conformations and dynamics will be described later.

To further understand polymer conformations in these systems, observations from MD simulations are compared to simple random walks generated in a similar environment. Specifically, smooth-walled NPs matching the size and location of NPs in the MD simulations were placed in space. Then, the starting location of the random walk was randomly generated and steps of 1σ were generated in random directions. All starting locations and subsequent steps beyond R_{NP} from the NP center were accepted and all locations and steps within the NP were declined except those within 1σ of the NP surface which were accepted conditionally. To be specific, an exponential function that dictates acceptance criteria was used near the NP surface (from R_{NP}-1 to R_{NP}) to match the amorphous NP surface structure, both of which lead to a slightly less sharp NP surface (Figure 1c). This yields qualitatively similar NP-polymer and NP-step interfacial profiles and shows good agreement at the chain-scale with MD simulations, as will be discussed later. To account for the absence of excluded volume in the random walk, the number of steps per chain (n) is selected to match the bulk R_g from MD simulations. For example, to compare MD simulations of polymers with N=50, we use random walks with n=83 to match the random walk R_g to the bulk polymer R_g of ~3.6σ.

Results

Polymer Conformations: Effect of Confinement

We first present calculations of the chain conformations at various locations in the simulation box. It is useful to describe the conformation of a polymer chain by reporting the component of R_g perpendicular to the nearest NP surface ($R_g^{\perp}$), which follows the radial symmetry imposed by the NPs. As presented by Starr et al.[12], $R_g^{\perp}$ is calculated using Equation 1:

$$\left(R_g^{\perp}\right)^2 = \frac{1}{N^2}\left\langle \sum_{i=0}^{N-1}\sum_{j=i+1}^{N}\left(\frac{\left(\vec{r_i}-\vec{r_j}\right)\cdot\left(\vec{r_i}+\vec{r_j}\right)}{\left|\vec{r_i}+\vec{r_j}\right|}\right)^2\right\rangle \qquad (1)$$

where r_i represents the location of bead i with respect to the center of the nearest NP, N is the number of beads in the chain, and the coordinate system was shifted to place the NP at the origin during the calculation. In bulk polymer, where there are no NPs, the origin of the simulation box is used in place of the center of the nearest NP.

Figure 2 shows spatially resolved and time-averaged maps of $R_g^{\perp}$ within the NP monolayer (x-y plane, top) and through the NP monolayer (x-z plane, bottom) for N=50 chains in PNCs with R_{NP}~R_g for three confining environments. The value of $R_g^{\perp}$ is normalized to $R_g^{\perp}$ far from the NP surface ($R_g^{\perp,\infty}$), which matches $R_g^{\perp}$ in bulk polymer. Using $ID/2R_g = 2$ in Figure 2 as an example, $R_g^{\perp}$ is compressed near the NP surface and unperturbed far from the NP. The perturbed polymer layer is uniform in thickness around the NP in both planes. As the confinement increases, that is the NP-NP separation distance is decreased, the perturbed layer area maintains the same thickness and eventually the perturbed layers of adjacent NPs begin to overlap ($ID/2R_g = 0.5$, Figure 2). In fact, nearly all conformations in the x-y plane are perturbed when $ID/2R_g = 0.5$ and none resemble bulk-like conformations. In the x-z plane the chain conformations significantly above and below the NP monolayer are bulk-like, while conformations between the NPs are compressed. Although we only

report $R_g^{\perp}$, our observations of chain flattening against the NP surface are also apparent in analysis of the 3-D or individual components of R_g or the root mean squared end-to-end distance, R_{ee}.

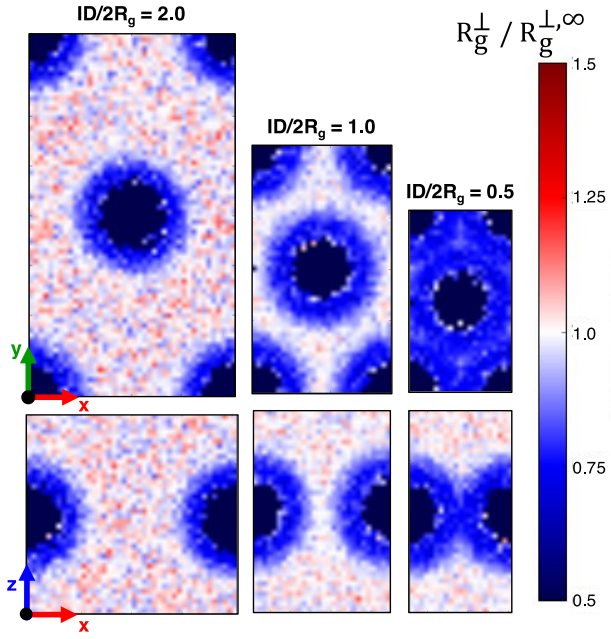

Figure 2: Maps of polymer conformations (N = 50, $2R_{NP} = 7\sigma$) plotted as $R_g^{\perp}/ R_g^{\perp,\infty}$ at three levels of confinement $ID/2R_g$ = 2, 1, and 0.5. (top) The x-z planes through the center of the NP monolayers. (bottom) The middle section of the x-z planes perpendicular to the NP monolayers which excludes the bulk regions far above and below the NP monolayer. The chain position is defined by the COM.

While Figure 2 illustrates the spatial influence of NPs and confinement on polymer conformation, Figure 3a presents the isotropically averaged conformations as a function of distance from the nearest NP surface. The positions of chains in this calculation were defined by their center of mass (COM) position from the NP surface normalized by R_g^{bulk}, $(r_{COM} - R_{NP})/R_g^{bulk}$. Consequently, it is possible for chains to wrap around the NP such that the COM is within the NP excluded volume without the presence of monomers within the excluded volume; this explains the apparent penetration into the NP in Figure 3a. The perpendicular component of the chain conformations at the NP surfaces, $R_g^{\perp}$, are ~ 25% smaller than the unperturbed conformation and mostly independent of confinement ($ID/2R_g$). In addition, we observe that polymers beyond ~R_g^{bulk} from the NP surface exhibit their bulk-

like conformation, similar to observations reported by Starr et al. on an isolated, faceted NP in a polymer melt of shorter polymer chains (N=20).[12]

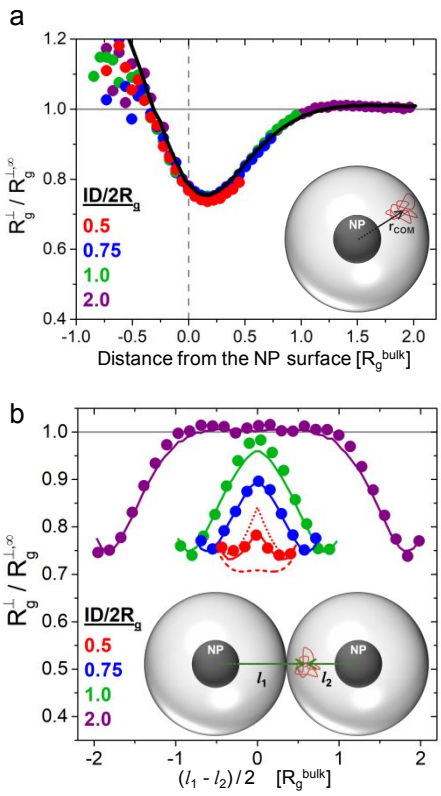

Figure 3: (a) Isotropically-averaged and normalized polymer conformation as a function of distance from the NP surface (defined by the chain COM). Symbols represent MD simulations and the solid line represents a random walk near an isolated NP. (b) Normalized polymer conformation as a function of COM position between two confining NPs. Symbols represent MD simulations and solid lines represent random walk generated in the same confining environment. At $ID/2R_g = 0.5$, the predicted perturbations considering only the nearest NP (dotted) and both confining NPs (dashed) are shown. All MD simulations are for N=50 and $2R_{NP} = 7\sigma$.

The analysis in Figure 3a restricts the maximum distance from the NP surface to be ID/2 to ensure an average around the nearest NP and it prevents double counting. In contrast, Figure 3b analyzes only the conformations in between nearest-neighbor confining NPs, as schematically represented in the inset. The x-axis, $(l_1 - l_2)/2$ in units of R_g^{bulk}, corresponds to the COM position relative to the midpoint between neighboring NPs where the midpoint is 0 and the minimum and max positions correspond to ID/2. Chains with COM inside the NP are excluded from Figure 3b for clarity.

When $ID/2R_g$ = 2 (purple), chains are compressed by 25% at the NP surface and exhibit bulk conformations when equidistant from neigbhoring NPs, as consistent with Figure 2. In contrast at $ID/2R_g$ = 0.5 (red), the most confined system has strongly perturbed chain conformations equidistant between the NPs.

It is interesting to note that the chain perturbations directly adjacent to the NPs are independent of confinement. This suggests that an isolated NP reasonably approximates the conformations at the NP-polymer interface regardless of confinement. When considering the perturbation beyond the NP surface and between neighboring NPs and comparing to an isolated NP, there are two limiting cases. First, the conformation of the polymer may be dictated by only the nearest NP. If this is true, the profile between NPs should follow the isotropically averaged profile observed in Figure 3a, which is represented by the dotted red line for $ID/2R_g$=0.5 in Figure 3b. This case underestimates the perturbation, indicating both NPs contribute to some degree to the perturbed conformation. The second limiting case is that both confining NPs perturb the chain conformation as much as the case of an isolated NP. Mathematically, this can be estimated by multiplying the perturbation at l_1 in Figure 3a by the perturbation at l_2. This case is represented by the dashed red line for $ID/2R_g$ = 0.5 in Figure 3b and clearly over estimates the perturbation. Thus, when $ID < 2R_g$, both confining NPs influence the conformation of the polymer chain, but their perturbations are not simply multiplicative.

To further probe conformations in these confining environments, we next compare the observed conformations to random walks in a similarly confined geometry, as described in the method section. The calculated conformations from random walks around an isolated NP are included as a solid line in Figure 3a. Even though the random walk uses a smooth NP and ignores self-excluded volume, it quantitatively captures the main observations from MD simulations. For example, conformations beyond R_g from the NP surface are bulk-like and conformations at the NP-polymer interface are flattened by ~25%. Using the same method, we now generate random walks in the confined environments between nearest-neighbor NPs and compare directly to MD simulations. For

all degrees of confinement, the observations using random walks (solid lines in Figure 3b) match those from MD simulations (points in Figure 3b). Thus, the flattened chain conformations are simply a result of confined random walks in these athermal PNC systems. The agreement between conformations from MD simulations and more facile random walk calculations was also observed in cylindrical[40] and thin film confinement[41]. The extension of this observation to conformations around spherical NPs, even when ID < $2R_g$, indicates that it can also be applied to more complex confining environments such as PNCs with various NP morphologies and filled porous media.

Polymer Conformations: Effect of Polymer Chain and NP size

We now explore the conformations of polymer chains with different chain lengths (N=50 and N=200) near NPs of different sizes ($2R_{NP}$ = 3.5, 7, and 14 s). In each case, R_{NP}/R_g is approximately 0.5, 1, or 2. Six NP monolayer systems were simulated corresponding to either $ID/2R_g$ = 0.5 or 1. Consistent with Figure 3, the isotropically-averaged and normalized polymer conformation is independent of $ID/2R_g$, Figure 4. Interestingly, the chain conformation profiles with matching R_{NP}/R_g collapse onto the same curve and systems with larger R_{NP}/R_g show larger perturbations near the NP interface. For example, when $R_{NP}/R_g \sim 0.5$, polymer conformations are relatively unperturbed, experiencing a ~5% decrease in $R_g^{\perp}$ when the chain COM is ~$0.5R_g$ from the surface of the NP. We also note that for each system, regardless of R_{NP}/R_g, the conformations begin to approach bulk-like values ~R_g from the NP surface. We observe the same effects using the random walk model, see Figure S3. This further supports the notion that conformations in complex confining environments and around various NPs, even when the NP and polymer have similar radii of curvature, are simply confined random walks.

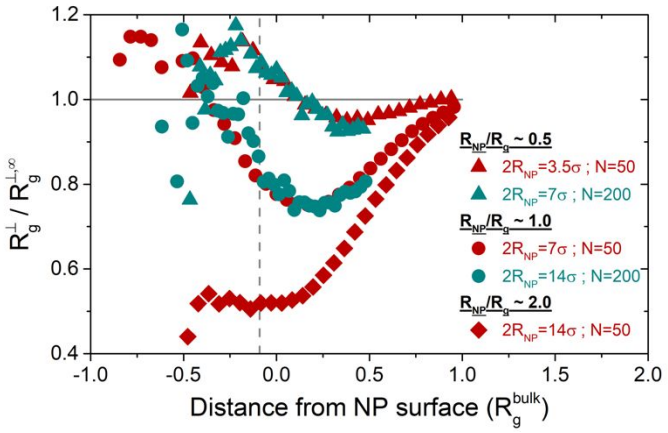

Figure 4: Isotropically-averaged and normalized polymer conformations as a function of COM distance from the NP surface showing the effect of NP size relative to bulk R_g (R_{NP}/R_g) for systems with different NP sizes and chain lengths. Triangles, circles, and diamonds represent R_{NP}/R_g = 0.5, 1.0, and 2.0, respectively. Systems with N=50 are shown in red and systems with N=200 are shown in teal.

Polymer Diffusion: Effect of Confinement

To probe polymer diffusion near and through confining NP monolayers, we begin by extracting the polymer chain diffusion coefficient in the z direction (D_z), perpendicular to the NP monolayer. The average D_z in the simulation box for N=50, $2R_{NP} = 7\sigma$, and $ID/2R_g = 0.5$ is 7.6×10^{-4} σ^2/τ, compared to bulk polymer which is 8.7×10^{-4} σ^2/τ, see Figure S4 and Table S1. This demonstrates that polymer diffusion is slower in systems with NPs. This 13% reduction in diffusion from this global average is noteworthy because the majority of the polymers in the simulation volume are more than R_g from the NP monolayer, yet polymer diffusion is still measurably perturbed. This demonstrates the spatially long-range impact of NPs on polymer diffusion, which was also reported in experiments. The monolayer geometry of these simulations facilitates more complex analyses to further probe this perturbation of chain scale dynamics, as described below.

To highlight the local polymer diffusion near and far from the NP monolayer, we compute the polymer diffusion coefficient as a function of distance from the NP monolayer. To be specific, we analyze monomer trajectories for time periods up to 60,000τ and for each trajectory and time period, calculate the average z position ($\bar{z}$), Figure 5a. Thus, $\bar{z}$ denotes the mean z position of the diffusing

species during a trajectory. The mean-squared displacement vs time curves in Figure 5b group monomers with similar $\bar{z}$ positions together, i.e. $10.5\sigma < \bar{z} < 17.5$. Each curve shows that MSD varies linearly with time at $t > \sim 30{,}000\tau$, indicating diffusive dynamics and providing the diffusion coefficient ($D = MSD/2t$). The MSD curves far from the NP monolayer ($\bar{z} > 17.5\sigma$) approach bulk polymer dynamics (solid line), while chain dynamics at smaller $\bar{z}$ are significantly suppressed relative to bulk diffusion or far from the NP monolayer.

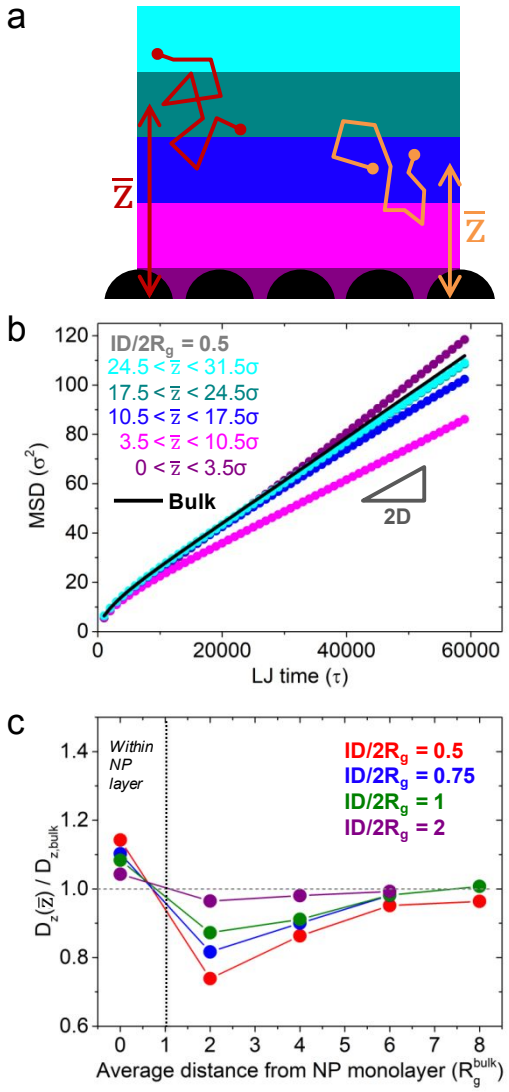

Figure 5: (a) Schematic representation of analysis to assign an average z position, $\bar{z}$, to a given monomer trajectory. (b) Time averaged mean-squared displacement as a function of time for various $\bar{z}$ ranges, as schematically represented in (a), for $ID/2R_g = 0.5$ (symbols) and bulk (solid line). (c) Normalized local polymer diffusion coefficient as a function of distance from the NP monolayer. These MD simulations used $N = 50$ and $2R_{NP} = 7\sigma$.

In Figure 5c, we summarize the spatial dependence of polymer diffusion by plotting the local z-directional diffusion coefficient, $D_z(\bar{z})$, normalized to D_z of bulk, as a function of the average distance from the NP monolayer, $\bar{z}$. Importantly, if we determine the system-average diffusion coefficient from this analysis by calculating a weight-average of $D_z(\bar{z})$ where the weight is the number of chains in each

binned $\bar{z}$, we recover the macroscopic D_z reported in Supporting Information. This self-check supports the validity of this local analysis and the attribution of a position to individual trajectories.

Independent of the levels of confinement ($ID/2R_g$), three regimes are evident as a function of distance from the NP monolayer: fast polymer diffusion within the NP monolayer, slow polymer diffusion just outside the NP monolayer, and bulk-like polymer diffusion far from the NP monolayer. For polymer diffusion within the NP monolayer ($\bar{z} < 1R_g^{bulk}$), Figure 5 shows that chains diffuse normal to the layer more rapidly than bulk. This result is reminiscent of the enhanced polymer diffusion observed under intermediate levels of confinement in athermal pores or between athermal substrates, where analogous systems exhibited $D/D_0 \sim 1.2$.[40–42] Furthermore, previous simulations of polymer diffusion in PNCs with smooth and repulsive NPs showed that diffusion near the NP surface is enhanced due to the reduced segmental friction near the NP.[18] In contrast to the enhanced diffusion within the NP monolayer, the strongest reduction in polymer diffusion is observed adjacent to the NP monolayer. For example, in the most confined case of $ID/2R_g=0.5$, diffusion at $\bar{z} \sim 2R_g$ is nearly 30% slower than bulk diffusion. Although less pronounced at larger $ID/2R_g$ values, a decrease in $D_z(\bar{z})/D_{z,bulk}$, is evident and likely associated with the tortuosity and reduced accessible volume of the confining NP monolayer. Finally, at long distances, diffusion within 5% of bulk is recovered in all systems.

Interestingly, a comparison of Figure 3a and 5c shows that the polymer conformations assume bulk behavior beyond $\sim R_g^{bulk}$ from the NP surfaces, while the slowing of chain-scale dynamics, namely the polymer diffusion coefficient, exists even at $\bar{z} \sim 6R_g^{bulk}$. The slower polymer diffusion resulting from the NP monolayer is clearly long-ranged. Note that the maximum MSD accessed in this calculation is $\sim 85 - 120\sigma^2$, corresponding to an average displacement of $\sim 10\sigma$ or $\sim 3R_g^{bulk}$. By comparison, the region over which diffusion is perturbed is more than 21σ or $\sim 6R_g^{bulk}$. This means that the NP monolayer perturbs polymer diffusion even when the average bead does not encounter the

NP monolayer, which makes the long-ranged slowing of polymer diffusion by the NP monolayer even more surprising. While a decoupling of dynamics and structure has been recently reported at the segment scale[43], our results strongly suggest that it extends to the chain-scale. This finding is consistent with the experimental results wherein polymer diffusion is slowed in PNCs even when ID is $>20R_g$[30] and qualitatively agrees with long-ranged perturbations measured in thin films[44].

Polymer Diffusion: van Hove Analysis

To further understand polymer diffusion through the NP monolayer, we calculate and analyze the one-dimensional van Hove distributions of polymer beads in the z direction. In this analysis, we calculate the probability (P) of finding a polymer bead at location z given a starting location (z_0) and lag time (Δt). The van Hove distribution for bulk polymer is shown in Figure 6a for three Δt. As expected, $P(z, \Delta t)$ in bulk follows a symmetric Gaussian distribution that broadens with increasing Δt. In fact, the variance of the distribution (Γ) increases with $\Delta t^{1/2}$ (Figure 6b) for $\Delta t > \sim 30{,}000\tau$, confirming diffusive motion with a diffusion coefficient matching $D_{z,bulk}$ (Figure S5).

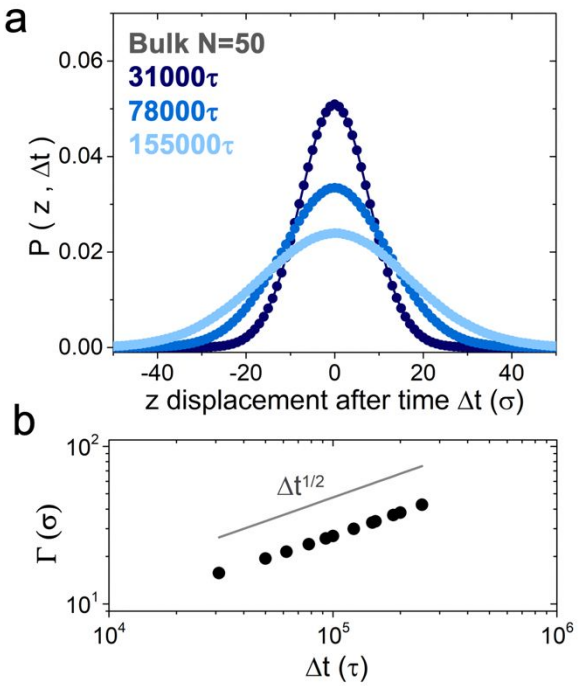

Figure 6: (a) Van Hove distributions of monomers in bulk polymer (N = 50) at three lag times, Δt. (b) Extracted variances (Γ) as a function of Δt showing diffusive behavior ($\Gamma \sim \Delta t^{1/2}$).

Figure 7a demonstrates the analysis for van Hove distributions in systems with NPs for initial bead locations just beyond the NP monolayer, $z_0 = 4\sigma$. We ascribe $z < 0$ to motion toward or through the NPs and $z > 0$ to motion away from the NPs. The distribution shown in dashed red in Figure 7a is the raw distribution which shows a clear depression in $P(z, z_0, \Delta t)$ in the NP monolayer ($z = -8\sigma - 0\sigma$) as a result of the decreased local volume fraction of polymer (Figure S2) . The solid red curve in Figure 7a represents the corrected van Hove distribution, obtained by dividing the raw distribution by the normalized local polymer volume fraction at each z position in the box and then renormalizing the distribution. The corrected van Hove distribution effectively accounts for the space occupied by the NPs but retains the dynamic information about the polymer motion. Additional examples of van Hove distributions at various z_0 (0, 4, 22σ) and $ID/2R_g$ (0.5, 1, 2) are presented in Figure S6.

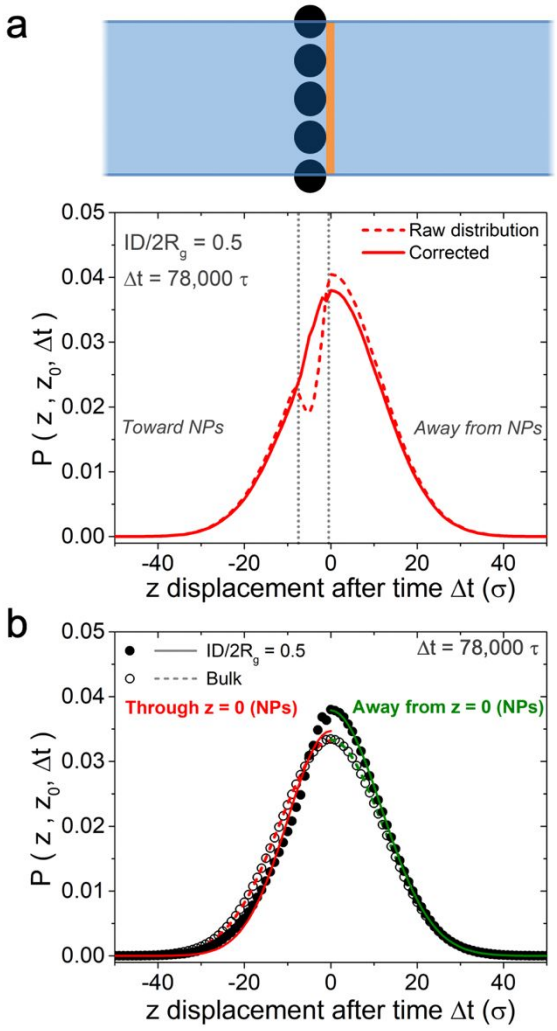

Figure 7: (a) Van Hove distribution of $ID/2R_g = 0.5$ for $\Delta t = 78{,}000\tau$ and corresponding schematic representation of the simulation box showing $z_0 = 4\sigma$ in orange. Dashed line represents the raw van Hove distribution and the corrected distribution obtained by dividing by the relative local polymer volume fraction. (b) Corrected van Hove distribution of $ID/2R_g = 0.5$ (solid symbols) compared to bulk (open symbols). Directional fitted Gaussian profiles are shown in red and green lines. MD simulations used $N = 50$ and $2R_{NP} = 7\sigma$.

The van Hove distributions of bulk polymer and $ID/2R_g$=0.5 are directly compared in Figure 7b. Although the maximum of each distribution is expectedly located at z = 0, the van Hove from the confined system is narrower and asymmetric relative to bulk. This observation means that diffusion

through the NP monolayer is slower than bulk, as expected from Figure 5c, and more chains diffuse away from the NP monolayer than through it. To further quantify this behavior, we use a piecewise Gaussian function to independently fit the distributions to the left and right while restricting the center to be at a z = 0; fits are included in Figure 7 for bulk (dashed) and confined (solid). The Gaussian fits are good, except for the distribution through the NP monolayer, which is likely due to the correction for polymer volume fraction (Figure S7). Even still, the two parameters extracted from these fits accurately capture the width (Γ) and integrated amplitude (amplitude) of all distributions, both of which are discussed separately below.

The widths of the distribution in each direction provide the diffusion coefficients, $D_z = \Gamma/(2t)$, toward and away from the NP monolayer. Figure 8 shows these diffusion coefficients normalized to the bulk as a function of confinement, $ID/2R_g$, and nanoparticle size, $2R_{NP}$. Diffusion away from the NP monolayer (green) remains within ~5% of bulk diffusion, while diffusion through the NP monolayer is ~40% slower under the most confined case. The trend for diffusion through the NP monolayer in Figure 8a is reminiscent of the functional form observed experimentally for bulk polymer nanocomposites[4,27] and an excluded volume model.[45] Of course, the magnitude of reduced diffusion is larger in experimental nanocomposites with randomly distributed athermal NPs throughout a polymer matrix, as compared to these simulations of only a single monolayer of athermal NPs.

Figure 8b highlights the effect of NP size at fixed N=50 and ID=1. While slow NP diffusion toward the NP monolayer and bulk-like diffusion away from the NP monolayer is observed regardless of NP size, we find that larger NPs slow diffusion toward the NP more strongly. This result is in agreement with recent MD simulations that show polymer diffusion in PNCs was more impacted by larger NPs.[36] While the slower diffusion observed through the monolayer may be impacted by excluded volume, it is also likely influenced by configurational entropy of the chains, as suggested experimentally.[32] Experimental results in weakly attractive PNCs over a narrower range in NP-size

suggest the normalized diffusion coefficient is largely independent of NP size at fixed $ID/2R_g$[28,29]. This apparent discrepancy between simulations and experiments indicates an opportunity for further investigation where systematic studies of the polymer COM diffusion coefficient as a function of R_{NP}, M_w, and ID in the regime of $R_g \sim R_{NP}$ and in the same material system may provide insights. We note that it is experimentally challenging to isolate each contribution to $ID/2R_g$ because changes in NP size, for example, may give rise to changes in dispersion state, NP mobility, and NP-polymer interactions. As a result, it may be useful to employ MD simulations more closely related to existing experimental systems and measurements.

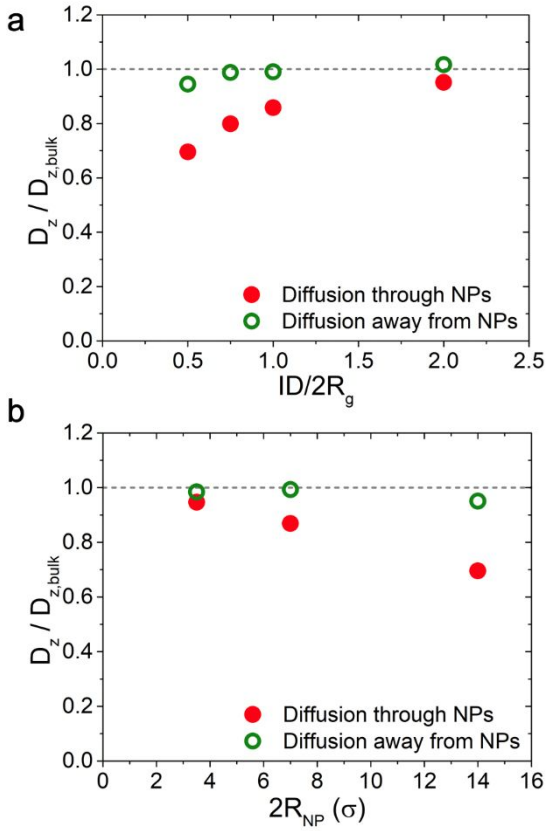

Figure 8: Normalized diffusion coefficient through (solid) and away from (open) the NP monolayers as a function of (a) $ID/2R_g$ and (b) $2R_{NP}$. Simulations in (a) used $N = 50$ and $2R_{NP} = 7\sigma$. Simulations in (b) used $N = 50$ and $ID/2R_g = 1$. The diffusion coefficients were averaged over six $\Delta t > 31{,}000\tau$ and errors are smaller than the size of data points.

To capture both the asymmetry and length scale of the perturbations imposed by the NP monolayer, we calculate the amplitudes of the van Hove distributions for beads diffusing through the NPs, P(z<0), and away from the NPs, P(z>0). Figure 9 plots the ratio of these values, P(z>0)/P(z<0), as a function of the starting location, $z_{0,}$ at $\Delta t = 78{,}000\tau$. Notably, this analysis refers to diffusion directions relative to the NP monolayer (rather than the simulation box), such that the simulation indeed has a net flux of zero through the NP monolayer. This analysis highlights the asymmetry due to geometric and tortuosity effects of the NP monolayer but does not reflect the diffusion rate (Figure 8). Figure 9 shows that more chains near the NP monolayer ($z_0 < \sim 3R_g$) diffuse away from the NP monolayer than chains that diffuse through it. This asymmetry in the number of diffusing chains is stronger for more confined systems. These findings are expected from excluded volume because fewer chains can enter the monolayer than diffuse away[27,46], but the shape and recovery of the symmetry beyond $\sim 3.5R_g$ is somewhat surprising.

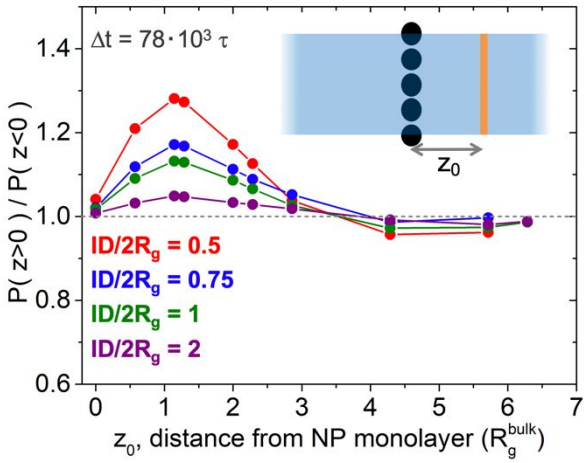

Figure 9: The ratio of the integrated van Hove distributions away from and through the NP monolayer, P(z>0)/P(z<0), as a function of the initial position, z_0. Simulations used N = 50 and $2R_{NP}=7\sigma$. The von Hove distributions correspond to $\Delta t = 78{,}000\tau$.

Overall, Figures 8 and 9 use the van Hove distributions to show that the monolayer of confining NPs slows diffusion toward the NPs without perturbing diffusion away and that more chains diffuse away from the layer than through it. While diffusion pathways in polymer nanocomposites will be more tortuous than the trajectories near the NP monolayers studied here, the hexagonally packed monolayers provide a well-defined local environment with independent control of ID and R_{NP} to highlight changes in polymer conformations and chain-scale dynamics in confinement.

Conclusion

We use coarse-grained molecular dynamics simulations to study polymer behavior in the presence of a monolayer of hexagonally packed NPs in a polymer melt with athermal interactions. Using this unique simulation box, we study the polymer conformations within the NP monolayer, analyze the spatial and temporal impact of the NP monolayer on polymer diffusion, and probe the transition from bulk to confined behavior in both cases.

Under strong confinement ($ID/2R_g < 1$) polymers are more impacted by two neighboring NPs than by an isolated NP and the magnitude of this effect increases with the ratio R_{NP}/R_g rather than either R_{NP} or R_g independently. Furthermore, we show that these conformations are consistent with a confined random walk, which provides a straightforward method for predicting conformations in complex confining environments. In systems with NP monolayers, polymer diffusion is slower than bulk and is most significant at large confinements (smaller $ID/2R_g$) and near the NPs. Although perturbations to the polymer conformations only persist to ~R_g from the NP monolayers, the slower polymer diffusion persists to ~$6R_g$. An analysis of the directional van Hove distributions shows that polymers preferentially diffuse away from the NP monolayer and diffusion through the NP monolayer is slowed relative to diffusion away from the NP monolayer. Remarkably, these simulations of straightforward NP monolayers capture the functional form observed experimentally in more complex

PNC environments, namely the normalized diffusion coefficient decreases with decreasing $ID/2R_g$. These molecular dynamics simulations highlight the impact of a monolayer of NPs and provide fundamental insights into the temporal and spatial effect of confining NPs on polymer conformations and diffusion. The observations from these simplified systems help provide context for more complicated PNC systems and help develop fundamental intuition to understand chain-scale polymer behavior in PNCs.

Associated Content

Supporting Information: Table of simulation parameters, polymer density plotted as a function of z position, conformation maps for random walk calculations at various ID, isotropically-averaged plots of conformations as a function of distance from the NP for random walk calculations at different R_g/R_{NP}, global MSD plots for different directions and confinements, time dependence of directional diffusion coefficient extracted from van Hove distributions, van Hove distributions for different z_0, and a log-linear plot of Gaussian fits to representative van Hove distributions.

Author Information

Corresponding Author:
* Email: winey@seas.upenn.edu (K.I.W.).

ORCID:
Eric J. Bailey: 0000-0001-7194-9035
Robert A. Riggleman: 0000-0002-5434-4787
Karen I. Winey: 0000-0001-5856-3410

Notes:
The authors declare no competing financial interest.

Acknowledgements

E.J.B., R.A.R., and K.I.W. gratefully acknowledge support from DOE BES DE-SC0016421. E.J.B. and K.I.W. also acknowledge support from ACS PRF 57405. E.J.B. acknowledges support from the National Science Foundation Graduate Research Fellowship Program under Grant DGE1321851. Computational resources were made available through XSEDE (TG-DMR-160115), which is

supported by National Science Foundation grant number ACI-1548562. Finally, the authors acknowledge James Pressly and Emily Lin for helpful discussions and assistance with simulations and analysis.

References

(1) Cheng, S.; Carroll, B.; Bocharova, V.; Carrillo, J. M.; Sumpter, B. G.; Sokolov, A. P. Focus: Structure and Dynamics of the Interfacial Layer in Polymer Nanocomposites with Attractive Interactions. *J. Chem. Phys.* **2017**, *146* (20), 203201/1-14.

(2) Lin, C. C.; Parrish, E.; Composto, R. J. Macromolecule and Particle Dynamics in Confined Media. *Macromolecules* **2016**, *49* (16), 5755–5772.

(3) Kumar, S. K.; Benicewicz, B. C.; Vaia, R. A.; Winey, K. I. 50th Anniversary Perspective: Are Polymer Nanocomposites Practical for Applications? *Macromolecules* **2017**, *50* (3), 714–731.

(4) Bailey, E. J.; Winey, K. I. Dynamics of Polymer Segments, Polymer Chains, and Nanoparticles in Polymer Nanocomposite Melts: A Review. *Prog. Polym. Sci.* **2020**, 101242.

(5) Kumar, S. K.; Ganesan, V.; Riggleman, R. A. Perspective: Outstanding Theoretical Questions in Polymer-Nanoparticle Hybrids. *J. Chem. Phys.* **2017**, *147* (2), 020901.

(6) Mackay, M. E.; Tuteja, A.; Duxbury, P. M.; Hawker, C. J.; Van Horn, B.; Guan, Z.; Chen, G.; Krishnan, R. S. General Strategies for Nanoparticle Dispersion. *Science (80-.).* **2006**, *311* (5768), 1740–1743.

(7) Jouault, N.; Crawford, M. K.; Chi, C.; Smalley, R. J.; Wood, B.; Jestin, J.; Melnichenko, Y. B.; He, L.; Guise, W. E.; Kumar, S. K. Polymer Chain Behavior in Polymer Nanocomposites with Attractive Interactions. *ACS Macro Lett.* **2016**, *5* (4), 523–527.

(8) Crawford, M. K.; Smalley, R. J.; Cohen, G.; Hogan, B.; Wood, B.; Kumar, S. K.; Melnichenko, Y. B.; He, L.; Guise, W.; Hammouda, B. Chain Conformation in Polymer Nanocomposites with Uniformly Dispersed Nanoparticles. *Phys. Rev. Lett.* **2013**, *110* (19), 1–5.

(9) Jouault, N.; Kumar, S. K.; Smalley, R. J.; Chi, C.; Moneta, R.; Wood, B.; Salerno, H.; Melnichenko, Y. B.; He, L.; Guise, W. E.; et al. Do Very Small POSS Nanoparticles Perturb S-PMMA Chain Conformations? *Macromolecules* **2018**, *51* (14), 5278–5293.

(10) Karatrantos, A.; Clarke, N.; Kröger, M. Modeling of Polymer Structure and Conformations in Polymer Nanocomposites from Atomistic to Mesoscale: A Review. *Polym. Rev.* **2016**, *56* (3), 385–428.

(11) Starr, F. W.; Schrøder, T. B.; Glotzer, S. C. Effects of a Nanoscopic Filler on the Structure and Dynamics of a Simulated Polymer Melt and the Relationship to Ultrathin Films. *Phys. Rev. E* **2001**, *64* (2), 021802/1-6.

(12) Starr, F. W.; Schrøder, T. B.; Glotzer, S. C. Molecular Dynamics Simulation of a Polymer Melt with a Nanoscopic Particle. *Macromolecules* **2002**, *35* (11), 4481–4492.

(13) Ndoro, T. V. M.; Voyiatzis, E.; Ghanbari, A.; Theodorou, D. N.; Böhm, M. C.; Müller-Plathe, F. Interface of Grafted and Ungrafted Silica Nanoparticles with a Polystyrene Matrix: Atomistic Molecular Dynamics Simulations. *Macromolecules* **2011**, *44* (7), 2316–2327.

(14) Liu, J.; Wu, Y.; Shen, J.; Gao, Y.; Zhang, L.; Cao, D. Polymer–Nanoparticle Interfacial Behavior Revisited: A Molecular Dynamics Study. *Phys. Chem. Chem. Phys.* **2011**, *13* (28), 13058.

(15) Goswami, M.; Sumpter, B. G. Anomalous Chain Diffusion in Polymer Nanocomposites for Varying Polymer-Filler Interaction Strengths. *Phys. Rev. E - Stat. Nonlinear, Soft Matter Phys.* **2010**, *81* (4), 1–8.
(16) Starr, F. W.; Schrøder, T. B.; Glotzer, S. C. Effects of a Nanoscopic Filler on the Structure and Dynamics of a Simulated Polymer Melt and the Relationship to Ultrathin Films. *Phys. Rev. E. Stat. Nonlin. Soft Matter Phys.* **2001**, *64* (2 Pt 1), 021802.
(17) Huang, J.; Mao, Z.; Qian, C. Dynamic Monte Carlo Study on the Polymer Chain in Random Media Filled with Nanoparticles. *Polymer (Guildf).* **2006**, *47* (8), 2928–2932.
(18) Desai, T.; Keblinski, P.; Kumar, S. K. Molecular Dynamics Simulations of Polymer Transport in Nanocomposites. *J. Chem. Phys.* **2005**, *122* (13), 134910.
(19) Smith, G. D.; Bedrov, D.; Li, L.; Byutner, O. A Molecular Dynamics Simulation Study of the Viscoelastic Properties of Polymer Nanocomposites. *J. Chem. Phys.* **2002**, *117* (20), 9478–9490.
(20) Dionne, P. J.; Ozisik, R.; Picu, C. R. Structure and Dynamics of Polyethylene Nanocomposites. *Macromolecules* **2005**, *38* (22), 9351–9358.
(21) Kutvonen, A.; Rossi, G.; Ala-Nissila, T. Correlations between Mechanical, Structural, and Dynamical Properties of Polymer Nanocomposites. *Phys. Rev. E* **2012**, *85* (4), 041803.
(22) Karatrantos, A.; Clarke, N.; Composto, R. J.; Winey, K. I. Polymer Conformations in Polymer Nanocomposites Containing Spherical Nanoparticles. *Soft Matter* **2015**, *11* (2), 382–388.
(23) Holt, A. P.; Griffin, P. J.; Bocharova, V.; Agapov, A. L.; Imel, A. E.; Dadmun, M. D.; Sangoro, J. R.; Sokolov, A. P. Dynamics at the Polymer/Nanoparticle Interface in Poly(2-Vinylpyridine)/ Silica Nanocomposites. *Macromolecules* **2014**, *47* (5), 1837–1843.
(24) Bailey, E. J.; Griffin, P. J.; Tyagi, M.; Winey, K. I. Segmental Diffusion in Attractive Polymer Nanocomposites: A Quasi-Elastic Neutron Scattering Study. *Macromolecules* **2019**, *52* (2), 669–678.
(25) Gong, S.; Chen, Q.; Moll, J. F.; Kumar, S. K.; Colby, R. H. Segmental Dynamics of Polymer Melts with Spherical Nanoparticles. *ACS Macro Lett.* **2014**, *3* (8), 773–777.
(26) Starr, F. W.; Douglas, J. F.; Meng, D.; Kumar, S. K. Bound Layers "Cloak" Nanoparticles in Strongly Interacting Polymer Nanocomposites. *ACS Nano* **2016**, *10* (12), 10960–10965.
(27) Gam, S.; Meth, J. S.; Zane, S. G.; Chi, C.; Wood, B. A.; Seitz, M. E.; Winey, K. I.; Clarke, N.; Composto, R. J. Macromolecular Diffusion in a Crowded Polymer Nanocomposite. *Macromolecules* **2011**, *44* (9), 3494–3501.
(28) Gam, S.; Meth, J. S.; Zane, S. G.; Chi, C.; Wood, B. A.; Winey, K. I.; Clarke, N.; Composto, R. J. Polymer Diffusion in a Polymer Nanocomposite: Effect of Nanoparticle Size and Polydispersity. *Soft Matter* **2012**, *8* (24), 6512–6520.
(29) Lin, C.; Gam, S.; Meth, S.; Clarke, N.; Winey, K. I.; Composto, R. J. Do Attractive Polymer − Nanoparticle Interactions Retard Polymer Diffusion in Nanocomposites? *Macromolecules* **2013**, *46*, 4502–4509.
(30) Choi, J.; Hore, M. J. A.; Meth, J. S.; Clarke, N.; Winey, K. I.; Composto, R. J. Universal Scaling of Polymer Diffusion in Nanocomposites. *ACS Macro Lett.* **2013**, *2* (6), 485–490.
(31) Choi, J.; Hore, M. J. A.; Clarke, N.; Winey, K. I.; Composto, R. J. Nanoparticle Brush Architecture Controls Polymer Diffusion in Nanocomposites. *Macromolecules* **2014**, *47* (7), 2404–2410.
(32) Tung, W. S.; Griffin, P. J.; Meth, J. S.; Clarke, N.; Composto, R. J.; Winey, K. I. Temperature-Dependent Suppression of Polymer Diffusion in Polymer Nanocomposites.

ACS Macro Lett. **2016**, *5* (6), 735–739.
(33) Bailey, E. J.; Griffin, P. J.; Composto, R. J.; Winey, K. I. Multiscale Dynamics of Small, Attractive Nanoparticles and Entangled Polymers in Polymer Nanocomposites. *Macromolecules* **2019**, *52* (5), 2181–2188.
(34) Karatrantos, A.; Composto, R. J.; Winey, K. I.; Kröger, M.; Clarke, N. Modeling of Entangled Polymer Diffusion in Melts and Nanocomposites: A Review. *Polymers (Basel)*. **2019**, *11* (5), 876/1-29.
(35) Karatrantos, A.; Composto, R. J.; Winey, K. I.; Clarke, N. Polymer and Spherical Nanoparticle Diffusion in Nanocomposites. *J. Chem. Phys.* **2017**, *146* (20), 203331.
(36) Zhang, H.; Sun, D. D.; Peng, Y.; Huang, J. H.; Luo, M. B. Diffusivity and Glass Transition of Polymer Chains in Polymer Nanocomposites. *Phys. Chem. Chem. Phys.* **2019**, *21* (41), 23209–23216.
(37) Kremer, K.; Grest, G. S. Dynamics of Entangled Linear Polymer Melts : A Moleculardynamics Simulation Dynamics of Entangled Linear Polymer Melts : A Molecular-Dynamics Simulation. *J. Chem. Phys.* **1990**, *92* (8), 5057.
(38) Plimpton, S. Fast Parallel Algorithms for Short-Range Molecular Dynamics. *Journal of Computational Physics*. 1995, pp 1–19.
(39) Griffin, P. J.; Bocharova, V.; Middleton, L. R.; Composto, R. J.; Clarke, N.; Schweizer, K. S.; Winey, K. I. Influence of the Bound Polymer Layer on Nanoparticle Diffusion in Polymer Melts. *ACS Macro Lett.* **2016**, *5* (10), 1141–1145.
(40) Pressly, J. F.; Riggleman, R. A.; Winey, K. I. Polymer Diffusion Is Fastest at Intermediate Levels of Cylindrical Confinement. *Macromolecules* **2018**, *51* (23), 9789–9797.
(41) Pressly, J. F.; Riggleman, R. A.; Winey, K. I. Increased Polymer Diffusivity in Thin-Film Confinement. *Macromolecules* **2019**, *52* (16), 6116–6125.
(42) Tung, W. S.; Composto, R. J.; Riggleman, R. A.; Winey, K. I. Local Polymer Dynamics and Diffusion in Cylindrical Nanoconfinement. *Macromolecules* **2015**, *48* (7), 2324–2332.
(43) Zhang, W.; Emamy, H.; Pazmiño Betancourt, B. A.; Vargas-Lara, F.; Starr, F. W.; Douglas, J. F. The Interfacial Zone in Thin Polymer Films and around Nanoparticles in Polymer Nanocomposites. *J. Chem. Phys.* **2019**, *151* (12), 124705/1-9.
(44) Sauer, B. B.; Zheng, X.; Rubinstein, M.; Rafailovich, M. H.; Schwarz, S. A.; Sokolov, J.; Strzhemechny, Y. Long-Range Effects on Polymer Diffusion Induced by a Bounding Interface. *Phys. Rev. Lett.* **2002**, *79* (2), 241–244.
(45) Meth, J. S.; Gam, S.; Choi, J.; Lin, C. C.; Composto, R. J.; Winey, K. I. Excluded Volume Model for the Reduction of Polymer Diffusion into Nanocomposites. *J. Phys. Chem. B* **2013**, *117* (49), 15675–15683.
(46) Maxwell, J. C. *A Treatise on Electricity and Magnetism*; Oxford University Press: London, 1873.

Polymer Conformations and Diffusion Through a Monolayer of Confining Nanoparticles

SUPPORTING INFORMATION

Eric J. Bailey[1], Robert A. Riggleman[2], and Karen I. Winey*[1,2]

[1]Department of Materials Science and Engineering and [2]Department of Chemical and Biomolecular Engineering, University of Pennsylvania, Philadelphia, Pennsylvania 19104, United States

*Author to whom correspondence should be addressed. Electronic address: winey@seas.upenn.edu

I. Table of Simulation Parameters

Table S1: Table of simulations parameters including chain length (N), NP size ($2R_{NP}$), box dimensions (L_x, L_y, L_z), macroscopic diffusion coefficient in z direction (D_z), and the maximum LJ time.

Confinement	**N**	**$2R_{NP}$**	**R_g/R_{NP}**	**Lx**	**Ly**	**Lz**	**D_z**	**LJ time**
Bulk	50	N/A	N/A	22.744	22.744	22.744	8.7E-4	8.3E6
0.5	50	7	1	21.2	18.36	57.566	7.6E-4	1.7E7
0.75	50	7	1	24.8	21.48	42.167	7.7E-4	7.8E6
1	50	7	1	28.4	24.6	57.4	8.2E-4	1.2E7
2	50	7	1	21.4	37.07	47.4	8.5E-4	9E6
1	50	14	0.5	21.4	18.53	53.9	--	4.8E6
1	50	3.5	2	21.2	36.72	56.1	--	5.4E6

II. Polymer Density in Simulation Box

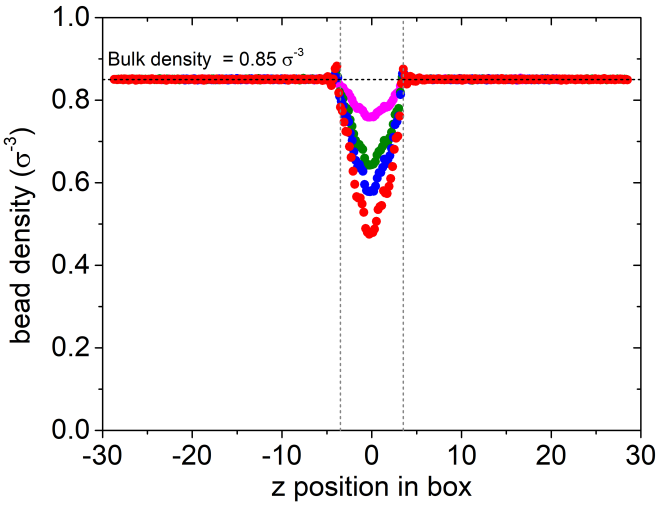

Figure S1: Local polymer density as a function of z position in the simulation box. Data presented are for N=50 and $2R_{NP}$= 7σ. Colors represent different levels of confinement: $ID/2R_g$ = 0.5 (red), 0.75 (blue), 1 (green), and 2 (magenta).

III. Random-walk Conformation Maps

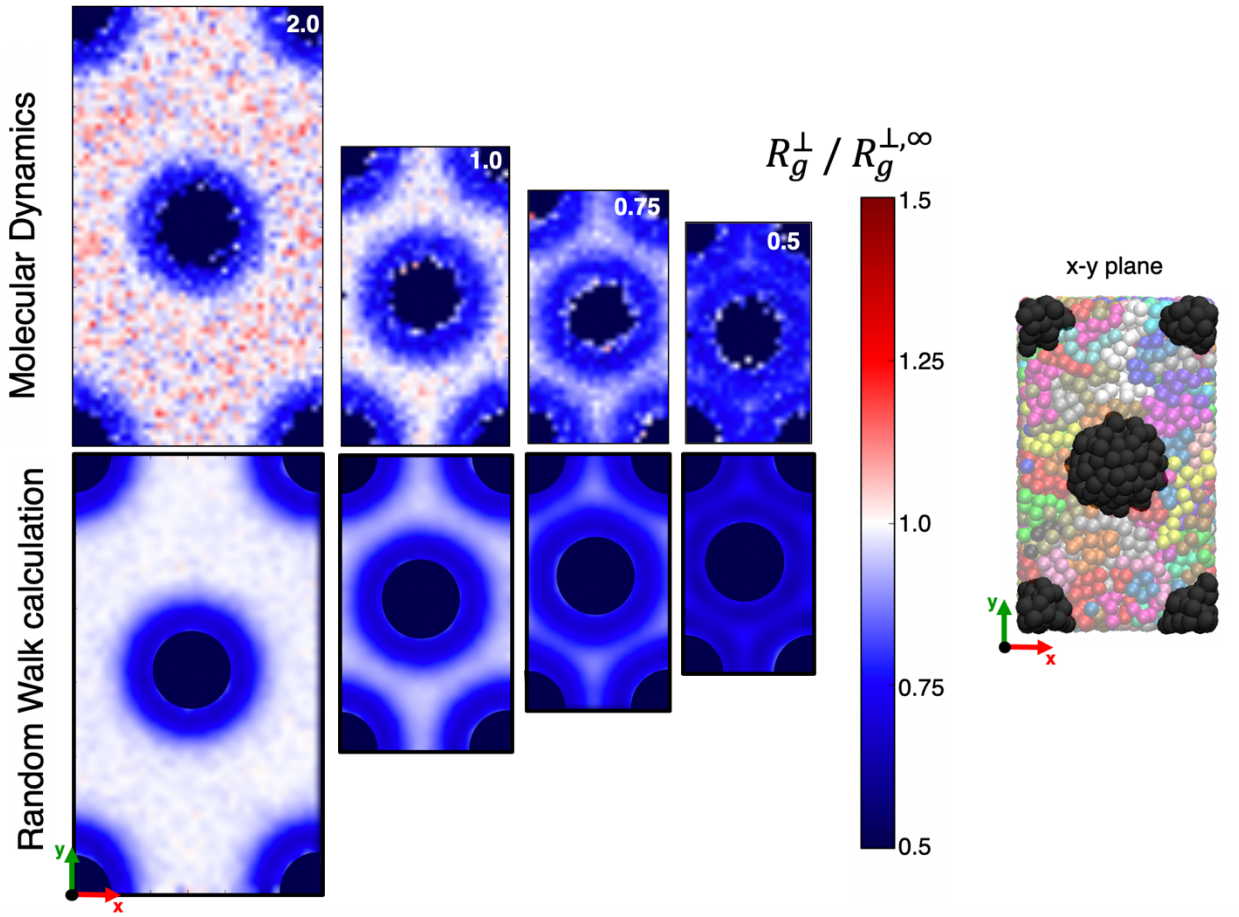

Figure S2: Conformation maps in x-y plane through NP monolayer for various degrees of confinement ($ID/2R_g$) obtained from MD simulations (top) and random walk calculations (bottom). NP representations in maps exclude conformations where the COM of the conformation is within the NP excluded volume. Data plotted are for $2R_{NP} = 7\sigma$ ($\sim 2R_g$) and N=50 for MD and n = 83 for random walk calculations.

IV. Random-walk Conformations Around NPs

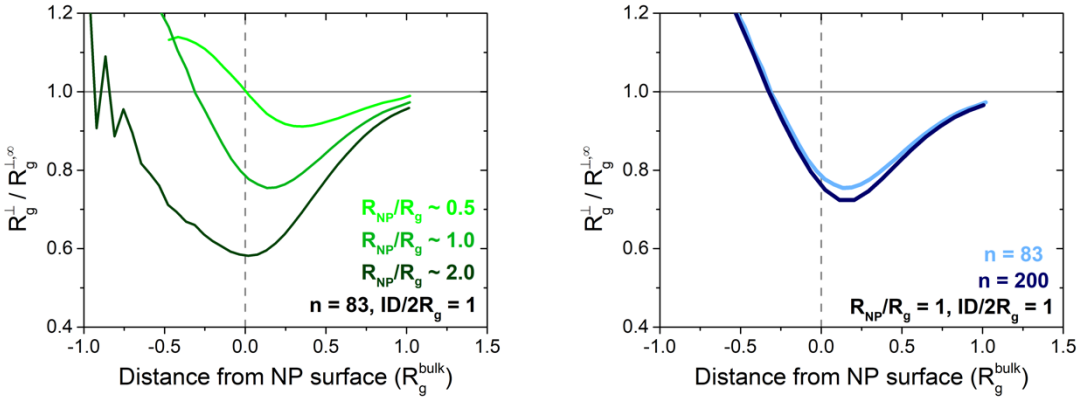

Figure S3: Conformation profile plotted as normalized perpendicular component of R_g as a function of COM distance from the NP surface (in units of R_g) for different NP sizes (left) and chain lengths (right).

V. MSD of Bulk and PNC systems

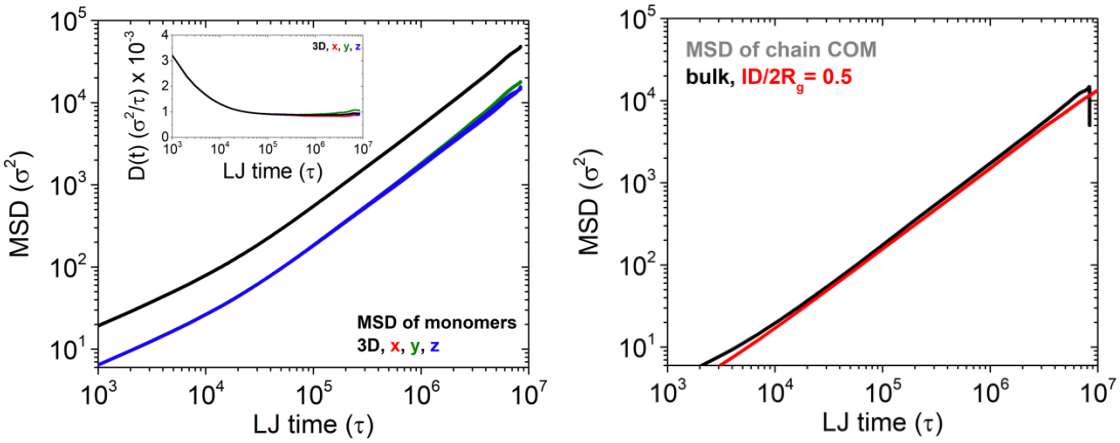

Figure S4: Macroscopic mean-squared displacement as a function of LJ time for bulk N=50 chains (left). Comparison of MSD in z-direction for N=50 chains in bulk and ID/$2R_g$=0.5 with $2R_{NP} = 7\sigma$ (right).

VI. Diffusion Coefficient extracted from van Hove Distribution as a function of time

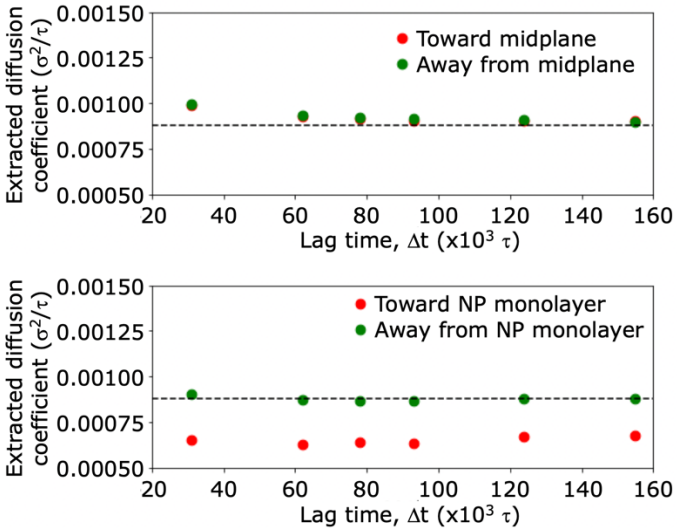

Figure S5: Extracted diffusion coefficient from van Hove distribution analysis as a function of time for bulk polymer (top) and ID/$2R_g$ = 0.5 (bottom) for N=50 chains, $2R_{NP} = 7\sigma$, and $z_0 = 4\sigma$. Dashed lines represent macroscopic diffusion coefficient of bulk polymer. In bulk, the diffusion coefficient toward and away from the midline (i.e. where the NPs reside when they are present) overlap as expected and both equal the macroscopic diffusion coefficient. When the NP monolayer is present, the diffusion coefficient toward the NP monolayer is lower than both away from the NP monolayer and the bulk value, as discussed in the text.

VII. van Hove Distributions for representative z_0

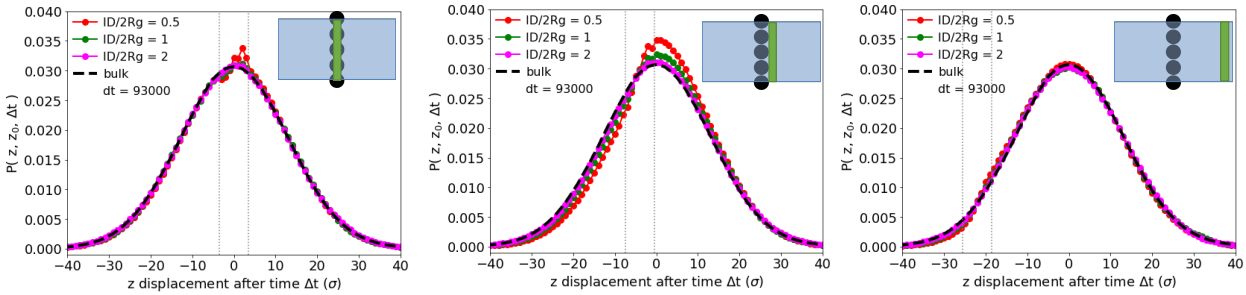

Figure S6: Van hove distributions for bulk and confined systems for several starting locations, as depicted in the insets, and $\Delta t = 93{,}000\tau$. Figures include $z_0 = 0$ (left), $z_0 = 4$ (middle), and $z_0 = 22$ (right), are obtained from systems with N=50 and $2R_{NP} = 7\sigma$, and are corrected for the NP volume as discussed in the main text.

VIII. Fitting of van Hove Distributions

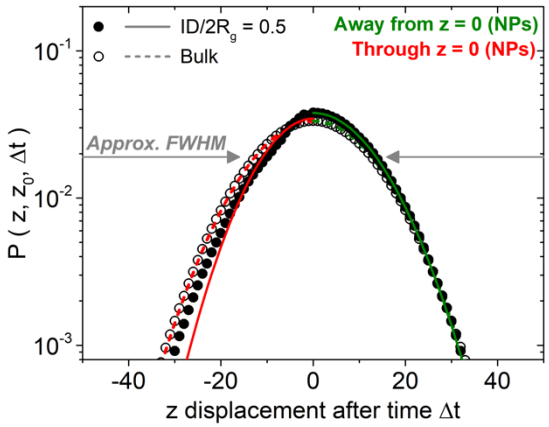

Figure S7: Corrected van Hove distribution of ID/2R_g = 0.5 (solid symbols) compared to bulk (open symbols) replicated from Figure 7b of the manuscript but plotted with a log y-axis. Directionally fitted Gaussian profiles are shown in red and green lines. MD simulations used N = 50 and $2R_{NP} = 7\sigma$. Both fits to bulk and the fit away from the NP monolayer in the PNC accurately represent the data. Although the fit to PNC data through the NP monolayer underrepresents the data at long distances, it accurately captures the FWHM and area under the curve of the data set, as discussed in the manuscript.